JOURNAL OF PROPULSION AND POWER
Vol. 20, No. 1, January–February 2004

Unsteady Solid-Propellant Pressure Combustion Response Using a Piston Burner

B. Saarloos* and M. Q. Brewster†
University of Illinois at Urbana—Champaign, Urbana, Illinois 61801

A small-scale solid-propellant laboratory burner has been designed to operate under piston-driven oscillating conditions from 40–400 Hz and 300–900 kPa mean pressure, with 10% amplitudes. The device was used to investigate the burning-rate response of a wide-distribution, bimodal AP (2:200 μm)-HTPB (IPDI) composite propellant (MURI TKC#5b). Results show that mean pressure and exit temperature decrease with increasing frequency because of increased heat transfer associated with oscillatory gas motion. Propellant burning rate is calculated numerically from pressure, volume, and frequency data using mass and energy balances. The dynamic burning rate response appears to be nearly linear at low frequencies (<150 Hz) and increasingly nonlinear at higher frequencies because of an increasing combustion response magnitude with frequency and nearly constant relative pressure amplitude. In the range of frequencies determined to be most linear (40–150 Hz), the magnitude of the pressure-coupled frequency response ranges from 2 to 7 $\pm$ 1, with burning rate lagging pressure by 50–75 deg. The results demonstrate the potential for the piston burner to measure pressure frequency response at low frequencies and also to measure nonlinear dynamic burn rates over a range of frequencies at high spectral resolution within a single test. The results also demonstrate that nonlinear response can appear as spectral structure in the apparent linear response when the data are interpreted linearly.

Nomenclature

A	=	area
A_b	=	burning area
C_D	=	nozzle discharge coefficient
c_p	=	specific heat
H	=	nondimensional heat loss
h	=	enthalpy, J/kg; heat-transfer coefficient
k	=	thermal conductivity
m	=	mass
$\dot{m}$	=	mass flow rate
Nu	=	Nusselt number
P	=	pressure
$\dot{Q}$	=	heat loss rate, W
R	=	mass-specific gas constant
R_p	=	pressure-coupled frequency response
Re	=	Reynolds number
r_b	=	burning rate
$\bar{S}_p$	=	mean piston speed
T	=	temperature
t	=	time
V	=	volume
γ	=	ratio of specific heats
θ_P, θ_T	=	phase angles
μ	=	gas viscosity
ρ	=	gas density
Ω	=	nondimensional frequency

Superscripts

-	=	mean
$'$	=	amplitude relative to mean

Received 18 June 2002; revision received 10 July 2003; accepted for publication 5 August 2003.

*Graduate Research Assistant, Department of Mechanical and Industrial Engineering.

†Hermid G. Soo Professor of Mechanical Engineering, Department of Mechanical and Industrial Engineering. Associate Fellow AIAA.

Introduction

THE unsteady combustion response of burning propellant to pressure fluctuations in a solid rocket motor is an important factor in determining the performance of the motor, including the ignition and tail-off transients as well as stability to perturbations during nominal burning. In the development and design of a solid-propellant rocket motor, there is a need to evaluate the dynamic combustion stability of the motor design. In a stable motor random pressure perturbations that occur will dampen out. Conversely, an unstable motor will result in pressure perturbations that can grow in amplitude, with the potential for disastrous consequences such as exceeding the guidance-and-control limits of the vehicle or destruction of the rocket motor itself. To evaluate the stability of the motor, one needs to know how the propellant responds to oscillating pressure conditions over a range of frequencies. Both linear and nonlinear pressure combustion responses are important, but the former has been investigated much more extensively both experimentally and theoretically.

The linear pressure response is characterized by the pressure-coupled frequency response function R_p, which is defined as

$$R_P = \frac{\Delta r_b / \bar{r}_b}{\Delta P / \bar{P}} e^{i\theta_P} \tag{1}$$

where Δ denotes the oscillatory component amplitude and the overbar denotes the mean or time-averaged value. Although analytical and computational methods have been developed for estimating mean flow and acoustic behavior in a rocket chamber, satisfactory methods have not yet been developed for predicting the response of the propellant combustion to pressure and velocity oscillations. Thus, obtaining this necessary data relies on laboratory test methods.

A variety of techniques[1–3] has been developed for measuring pressure-coupled response. These techniques can be divided into two categories—direct and indirect. Indirect techniques include the T-burner,[4–8] modulated exhaust jet burner,[2] and rotating valve.[2] These techniques use an indirect acoustic analysis to model the unsteady gas dynamics and combustion within the chamber. They require an analysis of unsteady gas dynamics during combustion in order to relate the propellant response function to the measured pressure. Thus, the deduced propellant response is only as accurate as the assumed model for the physical processes occurring within the chamber.

The T-burner, or center-vented burner, was the first method developed for measuring R_p and is still in use. The method uses an acoustic resonator tube that is typically $\frac{1}{3}$ to several meters in length and several centimeters in diameter, with propellant burning at both ends. The frequency of the test is directly related to the length. There are a few limitations of the T-burner, including expense and time required for testing, the fact that only one frequency data point is obtained per test, and uncertainties in the data-reduction analysis. It is also difficult to get low-frequency data because such long tubes are required that heat losses become significant. Attempts to overcome some of these limitations have led to alternative burner designs and to the development of new regression-rate measuring techniques.

Direct techniques include the microwave burner,[2] ultrasonic echoing,[9] and magnetic flowmeter.[10] These techniques all directly measure burning rate or gas velocity by different means. In the case of ultrasonic echoing and the microwave burner, waves are transmitted through the solid propellant. The instantaneous measurement of the phase shift between incident and reflected waves is directly proportional to the thickness of the propellant sample. The time derivative of the phase shift gives the unsteady burning rate.[2] One difficulty facing these techniques is how to deal with a propellant surface that is not uniform. Surface roughness is important because the distance-change resolution required for burn-rate measurement is of the same order of magnitude as the surface roughness.

The magnetic flowmeter technique is based on a gas-phase measurement rather than the solid regression rate. One measures the one-dimensional acoustic gas velocity as a function of the height above the propellant surface. The unsteady velocity is measured externally by imposing a strong magnetic field in a region containing the propellant surface. The combustion product gas has sufficient ionization to be electrically conductive and thus generates an electric potential proportional to the gas velocity. The instantaneous velocity combined with an instantaneous pressure allows a response function to be determined directly without reliance on an acoustic model.[10]

The direct methods all use some type of modulated exhaust at the nozzle exit in order to induce pressure oscillations within the chamber. One issue with this technique is that the amplitude of the unsteady signals is directly related to the modulation frequency. The amplitude of the pressure oscillation decreases with increasing frequency. At some point a frequency limit is reached where the unsteady component amplitude becomes of the same order as electronic noise and stochastic burning rate and pressure fluctuations. There is also a limitation with direct methods because of the fact that one is measuring intrinsic parameters, such as the propagation-time variation or the complex coefficient of reflection, or the strength of the electric field generated by the combustion gases. The basic question is raised of what exactly is being measured.

Comparisons between results from the variety of response techniques[1,2] reveal that although occasionally for limited data agreement has been shown, in general, when all available data are compared there is still significant disagreement among results by the various methods. Work is continuing to refine the various techniques, and in the future might lead to better agreement between techniques. In the mean time there remains a need for new pressure response measurement methods, both as a propellant/motor development tool, and as an unsteady combustion diagnostic for aiding in combustion theory advancement.

The goal of this research is the development of a technique for measuring a pressure combustion response that is quick, inexpensive, uses small propellant samples, and covers a wide frequency range in a single test with high spectral resolution. Achieving high spectral resolution is of particular interest in dealing with heterogeneous propellants to see how their response might deviate from the relatively smooth responses of homogeneous materials and to see if the strong spectral structure that has been observed in some laser-recoil response measurements[11] is also observed in pressure response when sufficient spectral resolution is available.

The basic technique of the experimental setup is to create forced pressure oscillations within the chamber by using a piston to oscillate the volume of the chamber while the propellant is burning. The advantages of the volume oscillatory setup include having direct control of the pressure oscillation frequency and the ability to ramp up the frequency in a short period of time to cover a range of frequencies in just one test. Another important characteristic is that unlike nozzle exhaust oscillation the amplitude of unsteady pressure does not change with frequency. Rather, it remains strictly a function of the mean pressure and the volume amplitude-to-mean ratio. This is generally an advantage.

In addition to changing frequency, the magnitude of the oscillation can also be changed by resizing the chamber volume and/or changing the piston displacement volume. Depending on the magnitude of the oscillations, the piston burner setup has the potential to measure both linear and nonlinear combustion frequency responses. This could prove very useful in validating dynamic propellant combustion models.

Apparatus and Procedure

A simplified schematic of the experimental apparatus is shown in Fig. 1. The important components are the removable nozzle, the side ports for measuring pressure and temperature, and the bottom ports that connect the combustion chamber to the piston chamber. The combustion chamber is 25 mm in diameter, with all other dimensions shown approximately to scale. The mean chamber volume with no propellant is $\bar{V} = 24$ cm^3. The displacement of the piston is 4.4 cm^3 such that the relative volume amplitude induced by piston motion is $\Delta V/\bar{V} = 2.2/24 = 9\%$ with no propellant. The apparatus is constructed entirely out of stainless steel, with the exception of the nozzle, which is made from copper to prevent destruction of the nozzle by the hot gases.

The piston assembly is a small single-cylinder model race car engine. The crankshaft is driven with a dc motor. The controller for the motor has a voltage-in signal that controls the speed of the motor. The oscillation frequency is ramped up and down using this voltage control.

Pressure measurements are taken at high frequency (10,000 Hz) using a piezoelectric quartz transducer installed in a water-cooled housing. The pressure is measured through one of the side ports shown in Fig. 1. A second pressure measurement is taken using a strain-gauge dc pressure transducer installed in another port. This transducer is isolated from the hot combustion gases using a tube filled with motor oil to act as a buffer between the hot combustion gases and the diaphragm of the transducer. This second pressure measurement is necessary to correct for a negative dc offset of the piezoelectric signal, which results from the rapid increase in chamber temperature. Temperature data are taken near the nozzle using a type-C tungsten-rhenium thermocouple.

The two pressure transducer signals are combined to construct the pressure trace for a given test. The high-frequency pressure transducer captures the ac component of the pressure and the low frequency of the dc component. A complete pressure trace is obtained

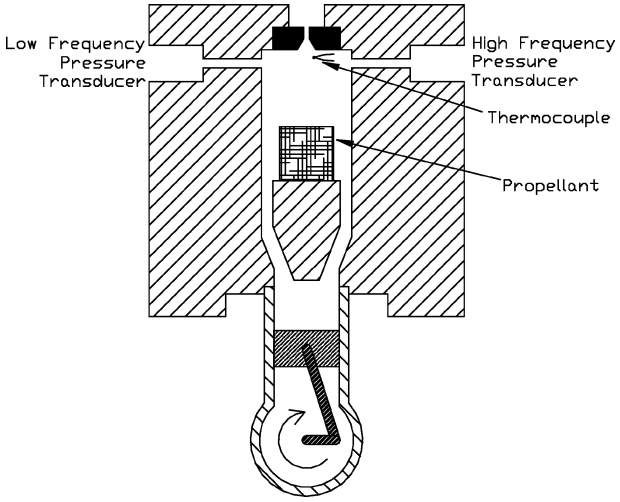

Fig. 1 Piston assembly and chamber schematic.

using a Butterworth low-pass digital filter on both signals. A Butterworth filter is chosen because it is maximally flat—it does not attenuate the magnitudes of the passed frequencies. A 25-Hz cutoff low-pass filter is applied to each signal. The low-pass signal of the strain gauge transducer becomes the mean or dc pressure component. The low-pass signal of the piezoelectric transducer is subtracted from the original signal, leaving the ac component of the pressure. The dc and ac components of pressure are then added together to give the complete pressure signal. Figure 2 shows the original pressure signals, their 25-Hz filtered signals, and the ac and dc components that are extracted. All pressure traces shown here were constructed in this manner.

The volume of the cylinder is tracked using an optical encoder mounted on the crankshaft. An index signal defines the starting position of the piston at the beginning of the test, and counting operations allow tracking of the relative position of the piston for the duration of the test. The counting operations also allow a speed (frequency) vs time signal to be constructed by measuring the number of rotations in a given period of time.

Propellant

The propellant used is an AP-composite propellant from Thiokol designated MURI-TKC#5b. It is a wide-distribution, bimodal AP (2 and 200 μm) and IPDI-cured HTPB mixture. Propellant samples are cut into rectangular cubes, typically with a height of 25–30 mm. Epoxy is used as an inhibitor for the surfaces of the propellant where burning is not desired. Ignition of the propellant is accomplished by use of a laser beam focused down through the nozzle and onto the propellant surface. A YAG laser of wavelength 1064 nm is used. Because the propellant is translucent to this wavelength, a boron-potassium nitrate igniter paste is spread across the top of the burning area to prevent in-depth heating and drilling into the propellant. The paste also helps to spread the flame quickly across the entire burning surface.

Steady Results

Steady, nonoscillatory tests were conducted first to experimentally verify targeted mean pressures. Figure 3 shows a typical steady test pressure and temperature trace. These tests showed that there is an initial slow rise in pressure, possibly caused by heat loss to a large initial free volume of room-temperature gas, as well as to cool chamber walls and nozzle surface. The nozzle-exit temperature for the steady tests stays quite constant for the duration of the test, although the temperature indicated by the thermocouple (~2000 K) is several hundred Kelvin below the adiabatic flame temperature (~2800 K). Thermocouple radiation loss can be shown to account for nearly all of the temperature discrepancy. In addition to radiation loss, the tungsten-rhenium thermocouple used oxidizes quickly in a combustion environment. Thus, the thermocouple data provide more of a qualitative description of temperature trends rather than a quantitative description of the actual temperature.

The nozzle size was varied between 1 and 2 mm according to the targeted mean pressure, which was typically 300–900 kPa. Such small nozzles were found to require analytical correction for boundary-layer viscous effects in calculating the mass discharged from the nozzle. Laminar boundary-layer equations were applied to the nozzle using the sonic properties of the gas. A sinusoidal velocity profile was assumed within the boundary layer,[12] integrated over the nozzle area and divided by the uniform velocity-area product to give a correction factor for the nozzle discharge coefficient C_D. This factor ranged from 0.7–0.99 depending on the nozzle size and gas properties. When this factor was applied in the mass balance equation, predicted pressures were within 10% (usually better) of measured steady pressures.

Simplified Linear Oscillatory Analysis

The general behavior of pressure and temperature under oscillating volume conditions with mass injection and expulsion can be obtained from a linear perturbation analysis on the chamber with

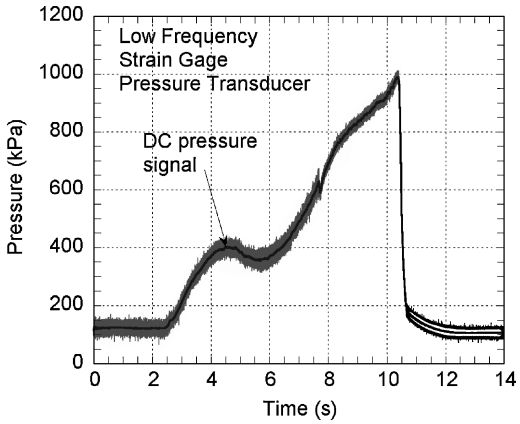

a) Filtered mean signal (dc)

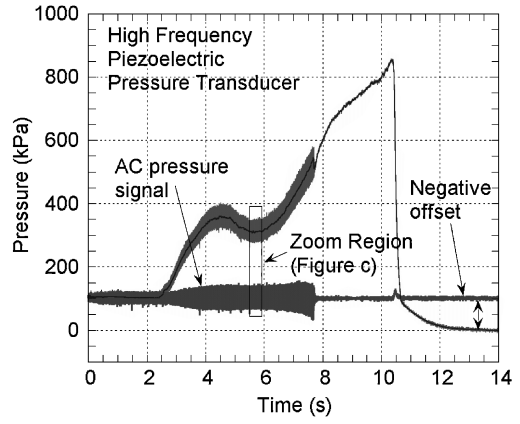

b) High-frequency signal

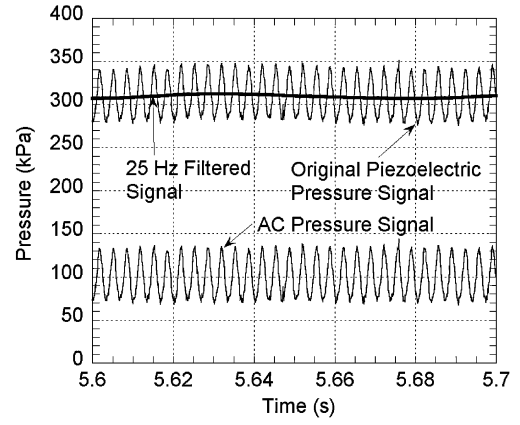

c) Time zoom of ac signal

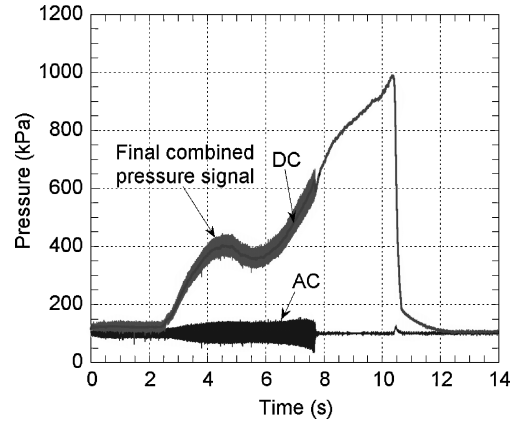

d) Combined dc and ac signals

Fig. 2 Construction of pressure signal.

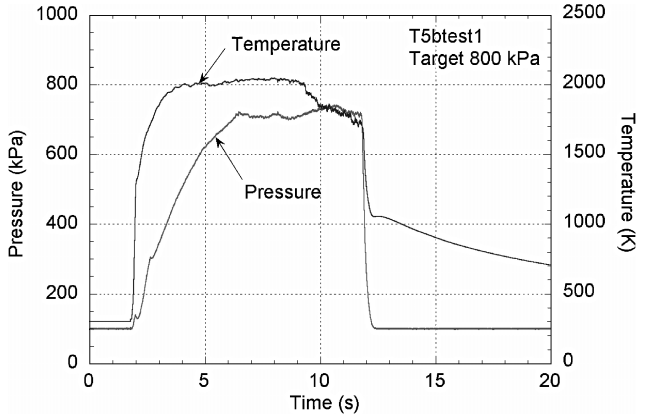

Fig. 3 Steady test exhibiting rise time to target pressure and nearly constant exit temperature.

constant mass injection rate. The analysis is based on the mass and energy equations:

(M):

$$\frac{\mathrm{d}m}{\mathrm{d}t} = \dot{m}_{\mathrm{in}} - \dot{m}_e \tag{2}$$

(E):

$$m\frac{\mathrm{d}h}{\mathrm{d}t} = \dot{m}_{\mathrm{in}}(h_{\mathrm{in}} - h) + V\frac{\mathrm{d}P}{\mathrm{d}t} - \dot{Q}_{\mathrm{out}} \tag{3}$$

where

$$\dot{m}_e = C_D A_t P \tag{4}$$

$$C_D = \sqrt{\gamma[2/(\gamma+1)]^{(\gamma+1)/(\gamma-1)}(1/RT)} = CT^{-\frac{1}{2}} \tag{5}$$

$$C = \sqrt{\gamma[2/(\gamma+1)]^{(\gamma+1)/(\gamma-1)}(1/R)} \tag{6}$$

Equations (5) and (6) assume choked flow, which was the condition for all data to which this analysis was applied. Substituting constant-composition ideal-gas relationships and a convective heat loss relation results in the following forms of the mass and energy equations:

(M):

$$\frac{1}{R}\left[\frac{P}{T}\frac{\mathrm{d}V}{\mathrm{d}t} + \frac{V}{T}\frac{\mathrm{d}P}{\mathrm{d}t} - \frac{PV}{T^2}\frac{\mathrm{d}T}{\mathrm{d}t}\right] = \dot{m}_{\mathrm{in}} - CT^{-\frac{1}{2}}A_t P \tag{7}$$

(E):

$$\frac{PV}{RT}c_p\frac{\mathrm{d}T}{\mathrm{d}t} = \dot{m}_{\mathrm{in}}c_p(T_{\mathrm{in}} - T) + V\frac{\mathrm{d}P}{\mathrm{d}t} - h_c A(T - T_w) \tag{8}$$

For simplicity, a spatially isothermal gas and constant mass injection rate are assumed. A linearized small perturbation oscillatory solution is assumed as follows:

$$V = \bar{V} + \Delta V e^{i\omega t} \tag{9}$$

$$P = \bar{P} + \Delta P e^{i(\omega t + \theta_P)} \tag{10}$$

$$T = \bar{T} + \Delta T e^{i(\omega t + \theta_T)} \tag{11}$$

Equations (9–11) are substituted into Eqs. (7) and (8), and $\mathcal{O}(\Delta^2)$ or higher terms are dropped. The equations can be further simplified by using the steady solution

(M):

$$\bar{P} = \frac{\dot{m}_{\mathrm{in}}}{C\bar{T}^{-\frac{1}{2}}A_t} \tag{12}$$

(E):

$$\bar{T} = \frac{\dot{m}_{\mathrm{in}}C_p T_{\mathrm{in}} + h_c A T_w}{\dot{m}_{\mathrm{in}}C_p + h_c A} \tag{13}$$

The characteristic time for the system to go from one steady state to another (when a parameter such as V or mass influx changes) is

$$\tau = 2\pi\bar{m}/\dot{m}_{\mathrm{in}} \tag{14}$$

and can be used to define a nondimensional frequency:

$$\Omega = \omega\bar{m}/\dot{m}_{\mathrm{in}} = (\bar{P}\bar{V}/R\bar{T})(\omega/\dot{m}_{\mathrm{in}}) \tag{15}$$

A nondimensional heat-transfer coefficient is defined as

$$H = h_c A/\dot{m}_{\mathrm{in}}c_p \tag{16}$$

Relative volume, pressure, and temperature amplitudes are

$$V' = \Delta V/\bar{V}, \qquad P' = \Delta P/\bar{P}, \qquad T' = \Delta T/\bar{T} \tag{17}$$

Substituting Eqs. (15–17) into Eqs. (7) and (8), using the constant-composition, ideal-gas specific heat and gas-constant relationship, and separating into real and imaginary parts yields

$$-P'\Omega\sin\theta_P + P'\cos\theta_P = -T'\Omega\sin\theta_T + \tfrac{1}{2}T'\cos\theta_T \tag{18}$$

$$\Omega V' + P'\Omega\cos\theta_P + P'\sin\theta_P = T'\Omega\cos\theta_T + \tfrac{1}{2}T'\sin\theta_T \tag{19}$$

$$\Omega T'\sin\theta_T = \Omega[(\gamma-1)/\gamma]P'\sin\theta_P + (H+1)T'\cos\theta_T \tag{20}$$

$$\Omega T'\cos\theta_T = \Omega[(\gamma-1)/\gamma]P'\cos\theta_P - (H+1)T'\sin\theta_T \tag{21}$$

Equations (18–21) can be solved for P'/V', T'/V', θ_P, and θ_T as functions of frequency Ω for given values of γ and H. Plots of these linear transfer function components are shown in Fig. 4 for $\gamma = 1.2$ and $H = 0$. The key parameter in determining the system response to volume fluctuations is the ratio of imposed oscillation frequency to system response frequency Ω. For $\Omega \ll 1$ the pressure and temperature amplitudes approach zero, corresponding to quasi-static behavior. For $\Omega \gg 1$ the pressure and temperature amplitudes approach nonzero constants and temperature and pressure both lag volume by 180 deg. In this case the linear analytic solution converges

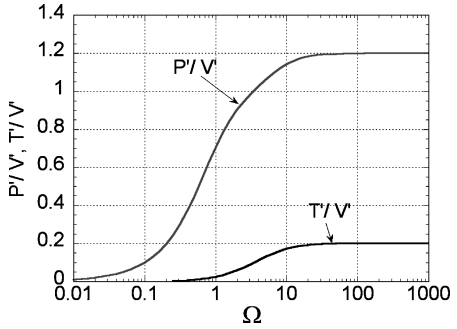

a) Relative amplitude ratios

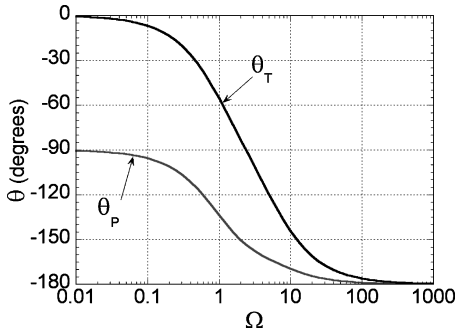

b) Phase angles

Fig. 4 Linearized oscillatory analysis with constant mass injection rate, no heat loss ($H = 0$), and $\gamma = 1.2$.

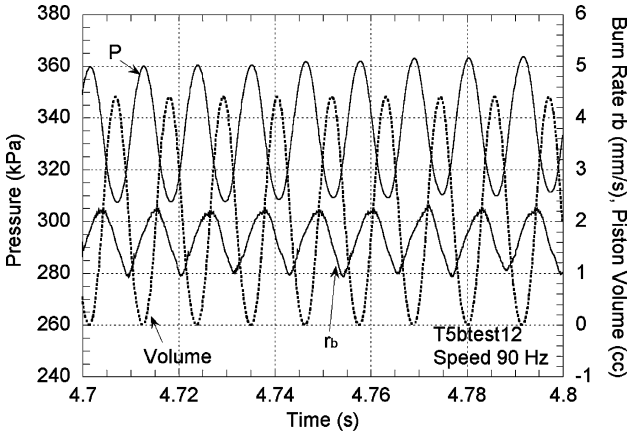

Fig. 5 Pressure, piston volume, and burning rate at low speed (90 Hz), exhibiting a nearly linear burning-rate waveform.

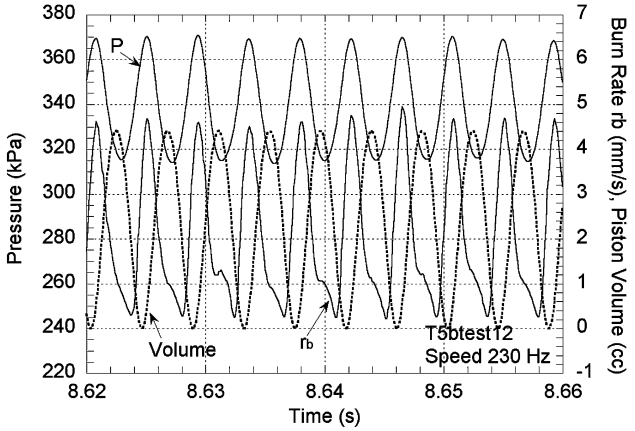

Fig. 6 Pressure, piston volume, and burning rate at medium speed (230 Hz) exhibiting a noticeably nonsinusoidal burning-rate waveform.

to the conditions of isentropic compression/expansion of a fixed-composition ideal gas in a closed volume with no mass injection or expulsion:

$$PV^{\gamma} = \text{constant}(\Omega \gg 1) \tag{22}$$

$$\mathrm{d}\,\ell_n P = -\gamma\,\mathrm{d}\,\ell_n V \rightarrow P'/V' = \gamma, \qquad \theta_P = -180 \text{ deg} \tag{23}$$

$$d\,\ell_n T = -(\gamma - 1)\,\mathrm{d}\,\ell_n V \rightarrow T'/V' = (\gamma - 1)$$

$$\theta_T = -180 \text{ deg} \tag{24}$$

In this limit pressure lags volume by 180 deg with an amplitude ratio of γ. Inert nitrogen injection tests confirmed these relations experimentally for the case of constant mass injection.

For conditions typical of an oscillatory propellant test, the characteristic frequency of the chamber ($1/\tau$) is about 7 Hz. The frequency of the piston oscillation (40–400 Hz) is much greater than the characteristic frequency of the chamber; Ω is in the high-frequency limit, varying from 6–60. Thus, it might be expected that the pressure–volume amplitude and phase relationships would, at least to a first approximation, be better represented by the high-frequency, closed-volume, isentropic relations, Eqs. (22–24), than the low-frequency, quasi-static limit. Such was indeed found to be the case (see discussion of Figs. 5–7).

Oscillatory Pressure Results

Figure 8 shows a typical result for pressure vs time for an oscillatory test with propellant burning. Ideally the oscillatory tests would have been conducted by igniting the propellant under constant volume–pressure conditions (to facilitate ignition), allowing the pressure to reach the target mean value, and then starting piston

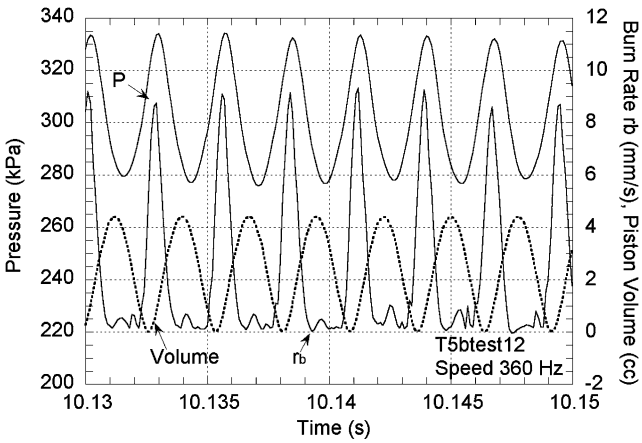

Fig. 7 Pressure, volume, and burning rate at high speed (360 Hz) exhibiting a nonlinear burning rate.

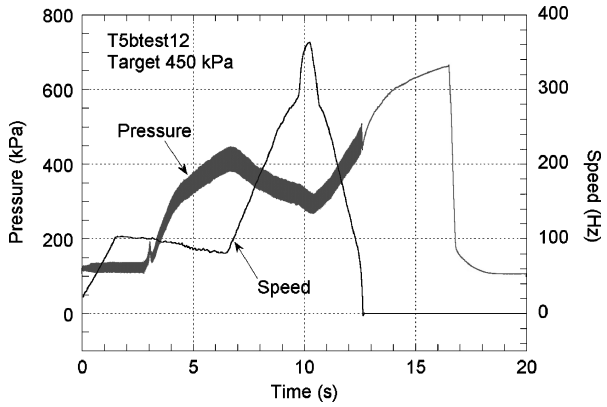

Fig. 8 Oscillatory test showing decreasing mean pressure with increasing oscillation frequency (speed).

motion to induce pressure oscillations. However, it was found that the torque required to start the piston moving against the chamber pressure was more than the dc motor could muster. To overcome this hurdle, the piston oscillation was started before the propellant was ignited. A leveling time was programmed into the speed-controlling voltage to allow the chamber to approach the target mean pressure before ramping of the piston speed was begun. As mean chamber pressure increased as a result of mass addition from burning propellant, the motor speed would drop slightly because of the additional work required. In Fig. 8 the motor speed was held at about 100 Hz until 7 s, allowing the mean pressure to reach 400 kPa. The mean pressure rise rate during the leveling time was noticeably slower than for a steady test because of heat transfer and oscillatory gas motion effects, as discussed next.

An unexpected and interesting phenomenon was observed during the oscillatory tests once the motor speed began ramping up: as shown in Fig. 8, the mean pressure began to decrease as the motor speed (oscillation frequency) began to increase. The mean pressure reached a minimum at the point of maximum speed. As motor speed was ramped down, the mean pressure began to increase again. When the oscillations stopped (speed = 0), the pressure rose to a level higher than at any point during the oscillations. It was found that this mean pressure behavior also correlated with temperature.

Figure 9 shows a plot of indicated gas temperature near the nozzle for a test that had a characteristic mean pressure variation similar to Fig. 8. A minimum in temperature occurs at the same time as for pressure, corresponding to maximum motor speed. This would explain the decrease in mean pressure as being caused by an increase in mean density of the cooler gas flowing through the nozzle, which increases the nozzle mass discharge rate. As with pressure, when the oscillations stop the temperature also rises to a level higher than at any point during the oscillations. The inverse dependence of mean

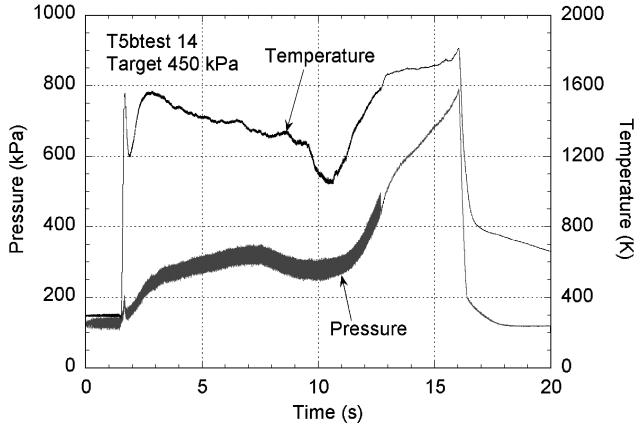

Fig. 9 Oscillatory test exhibiting minimum in exit temperature corresponding with minimum in mean chamber pressure.

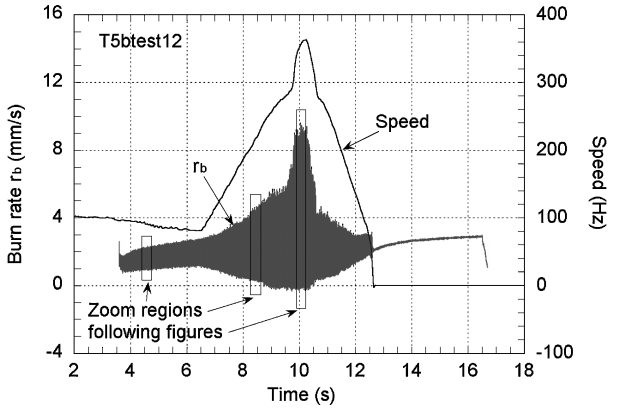

Fig. 10 Burning rate and speed vs time for the same test as Fig. 8, exhibiting increasing amplitude of burning-rate oscillation with increasing speed.

gas temperature on motor speed can be explained in terms of heat-transfer effects associated with the oscillating gas motion.

In any test, steady or oscillatory, there is significant heat loss from the combustion gases to the steel walls of the chamber and to the gas that was initially in the chamber. The rate of this heat loss is significantly exacerbated by oscillatory gas motions. Hot gas drawn into the side regions of the chamber by downward piston motion loses heat by radiation and convection to the walls as well as by mixing with surrounding cooler gas. This cooled mixture is then pushed back toward the nozzle when the piston moves up. The result is an exit gas temperature that oscillates with the piston motion and which, averaged over the piston cycle, decreases as piston speed increases. The average residence time of a fluid particle in the chamber for typical conditions as discussed earlier is approximately $\tau = 1/(7\text{ Hz}) = 0.15$ s. At an oscillation frequency of 200 Hz, an average fluid particle would experience about 200/7 or 30 oscillations during its lifetime in the chamber. Thus there is vigorous exchange of mass and energy between the hot gas regions near the burning surface and the cold gas regions away from the burning surface. The higher the oscillation frequency the greater the average heat loss and the lower the mean temperature of the gas exiting the nozzle, hence, the mean temperature and pressure trends exhibited in Figs. 8 and 9.

Burning Rate

Propellant burning rate was determined from the measured pressure and volume using the mass-energy framework described earlier. The combustion chamber was divided into four regions, and Eqs. (2) and (3) were applied to each. Gas mixture properties were obtained from complex chemical equilibrium calculations using JANNAF thermochemical data and ideal-gas mixing rules. Heat loss in the chamber was modeled using standard radiative and convective correlations. The chamber walls were assumed black with a temperature vs time relationship calculated from a heat-conduction analysis. Convective heat-transfer coefficients were calculated using an empirical relationship for piston-induced motion in internal combustion engines as adapted to the present configuration.[13] The relevant relationships are as follows:

$$Nu = hB/k = a \cdot Re^{0.7} \tag{25}$$

$$Re = \rho \bar{S}_p B/\mu \tag{26}$$

Here $\bar{S}_p$ is the mean piston speed defined by multiplying two times the stroke length by the frequency of oscillation and B is the bore diameter. The constant a generally varies with the intensity of charge motion and engine design ($0.35 \le a \le 0.8$). An intermediate value of $a = 0.6$ was used here based on comparison of compression ratios and operating speeds. The heat-transfer coefficient varied with motor speed and also with the temperature and properties of each region. Calculated exit temperatures were found to agree qualitatively with measurements in terms of decreasing mean with increasing frequency and quantitatively to within thermocouple radiation, lead-wire conduction, and degradation uncertainties.

Burning rate was found from

$$r_b = \dot{m}_{\text{in}}/\rho_s A_b \tag{27}$$

using a finite difference, time-marching numerical solution. As a check on the data-reduction scheme, the sum of the incremental burn rates multiplied by time step was verified to equal the initial height of the propellant sample. In addition to this, the inferred burning rate should never be less than zero. As it turned out, at the highest frequencies the burning-rate oscillations were very nonlinear in waveform with the inferred burning rate approaching zero. In the first attempts to model the process, the inferred burning rates at high frequency actually oscillated slightly below zero. This led to examination and refinement of modeling assumptions.

Figure 10 shows the derived instantaneous burning rate and oscillation frequency (speed) as a function of time for the same test as shown in Fig. 8. As frequency increases, so does the burning-rate amplitude. Figures 5–7 show a zoomed-in view of the volume, pressure and burning rate at low (90 Hz), medium (230 Hz), and high (360 Hz) speeds, respectively. The volume can be seen to be nearly (but not exactly) sinusoidal, a characteristic of piston engines. At all frequencies the pressure–volume relative amplitude ratio P'/V' is approximately the specific heat ratio γ. The volume relative amplitude ranges from 7 to 9%, and the resulting pressure relative amplitude from 8 to 11%, corresponding to γ of approximately 1.2, slightly higher than the expected value for the combustion gas composition. The phase relationship between P and V is approximately 180-deg lag at lower frequencies, but deviates noticeably from 180 deg at higher frequencies caused by the burning-rate response of the propellant. The burning rate at 90 Hz (Fig. 5) has a quasi-sinusoidal appearance, suggesting a nearly linear response at this frequency. (Actually there is a slight nonlinearity manifested, as discussed in connection with Fig. 11.) As frequency increases to 230–360 Hz (Figs. 6 and 7) the increasingly nonlinear waveform of the burning-rate response is evident. At 360 Hz the burning-rate amplitude is larger than at lower frequencies with a sharp peak nearly in phase with the pressure peak and a relatively flat bottom with very low burning rate during the low-pressure portion of the cycle.

Pressure Response Function

From the instantaneous burning rate and pressure data, a linear frequency response function of burning rate to pressure can be calculated based on the definition in Eq. (1). This was done using a digital Fourier transform (DFT). (If burning rate were measured independently of pressure, a cross-correlation technique would be preferable to reduce the influence of random noise, but in this case the burning rate is entirely dependent on the pressure signal; the coherence is perfect—albeit artificially so—and the question of reducing noise

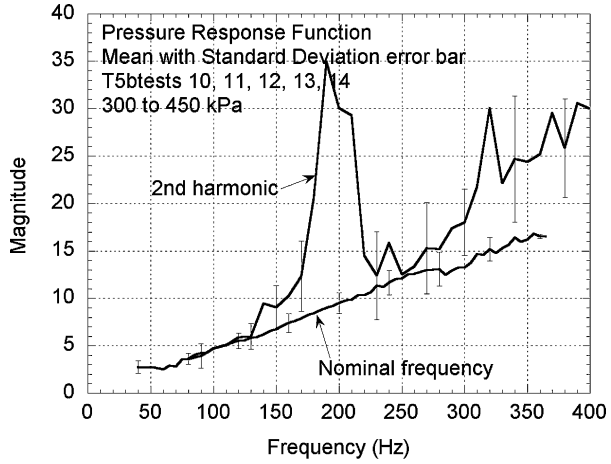

Fig. 11 Comparison of response function magnitude between second harmonic and fundamental frequency.

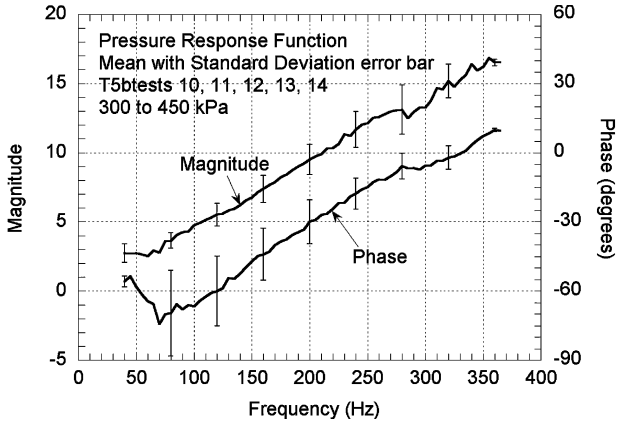

a) Magnitude and phase

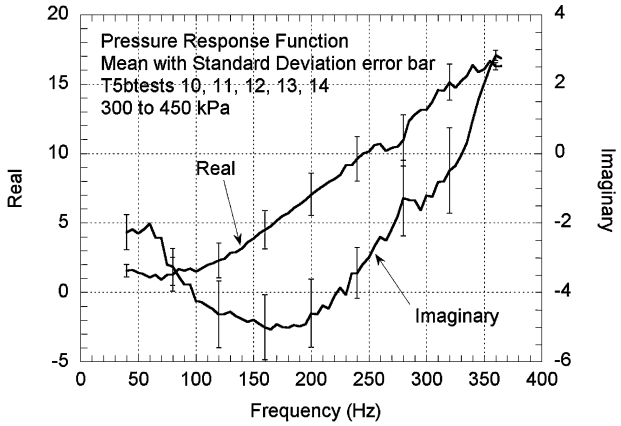

b) Real and imaginary parts

Fig. 12 Pressure-coupled response function.

is moot: Hence the straight DFT is adequate.) The pressure-coupled response function was thus obtained as

$$R_P = \frac{\mathrm{D}FT(r_b)}{\mathrm{D}FT(P)} \cdot \frac{\bar{P}}{\bar{r}_b} \tag{28}$$

Each test yielded two response function curves: one from the increasing frequency (ramp-up) portion of the test and one from the decreasing frequency (ramp-down) portion. The up and down curves from several tests were combined and averaged, giving the response function curves in terms of magnitude, phase, real and imaginary parts shown in Fig. 12.

The response magnitude (Fig. 12a) is 2.5–3 at 40–70 Hz, which seems physically plausible, and increases with frequency to surprisingly large values, for example, 15 at 320 Hz. One must wonder to what degree an indicated magnitude of 15 is physically meaningful. The trend with frequency is a partial check. Extrapolation of the general trend to zero frequency suggests a value that could be of the order of the steady-state pressure exponent, which for this propellant is approximately 0.5 at this pressure. The phase (Fig. 12a) is generally negative (lag) except above 330 Hz. At 70 Hz the phase reaches a minimum and begins increasing. This trend is also realistic because the phase must go to zero at zero frequency; one can imagine the phase in Fig. 12a continuing on the trend shown toward zero, or even going through a small positive region at frequencies below 20 Hz. (The estimated solid thermal relaxation or QSHOD frequency, below which the response usually manifests a positive phase, is about 20 Hz.) The in-phase or real part of the response (Fig. 12b) is between 1 and 2 from 40–120 Hz, which again seems plausible based on results from T-burners, which obtain the real part (only). As frequency increases, the indicated real part of the response increases to 15 at 320 Hz. Values this high are generally not seen with T-burner data. The present data are probably affected by the influence of nonlinear response, as discussed next. The imaginary part of the response shows mostly negative values with a minimum at 175 Hz and an increasing trend toward zero at zero frequency, as it should.

The question of the validity and implications of the calculated response function of Fig. 12 is considered next, particularly in light of the fact that at higher frequencies the burning rate appears to be nonlinear, yet the frequency response function is a linear concept (based on an assumed linear response). It was noted earlier that the burning-rate response of Fig. 7 at 360 Hz appeared nonlinear. This burning-rate data were filtered to obtain the fundamental component. As shown in Fig. 13, the 360-Hz component of this signal dips below zero, confirming that the response was indeed nonlinear (and not just the result of a large linear response to the small second harmonic component of the pressure wave, a possibility discussed further next). Although this procedure of checking for negative burning rate in the spectral components is one way of detecting nonlinear response, a finding of positive-definite spectral burning-rate components is not necessarily a guarantee of linear response. A more definite check of linearity would be to run experiments varying amplitude and check for independence from amplitude in the response. This would require a different piston displacement or mean volume, an experimental difficulty that we did not attempt. In lieu of that, we analyzed the data in a way that accomplishes the same objective without having to do additional experiments.

Advantage was taken of the fact that the volume oscillation of a piston-crank assembly is not perfectly sinusoidal. There is a second harmonic component to the volume input, with a magnitude about 10% that of the nominal (fundamental) frequency (i.e., a 150-Hz fundamental oscillation has a 300-Hz second harmonic component).

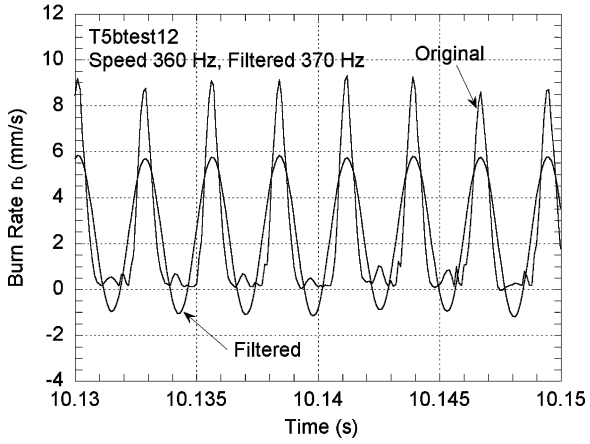

Fig. 13 Digital Fourier transform interpretation of nonlinear burning-rate data at the fundamental frequency of oscillation (360 Hz).

The resulting pressure oscillation also has a second harmonic component. Thus the response to the second harmonic can be isolated and calculated. Figure 11 compares the response function magnitude based on the fundamental frequency to that based on the second harmonic. The agreement is good—to within their standard deviations—up to 150 Hz. Above 150 Hz the second harmonic magnitude varies from the fundamental significantly and exhibits a large standard deviation. The second harmonic peak at 180 Hz, in contrast to the relatively flat fundamental response, is probably caused by a slightly nonlinear response when driven at 90 Hz (recall the r_b curve of Fig. 5) being exaggerated as an apparently large linear response to the small 180-Hz input component of the pressure wave by the linear DFT analysis. Theoretically, it is conceivable that the 180-Hz second harmonic peak is caused by a large linear response to the small second harmonic component of the pressure wave. But the fact that the response to the 180-Hz fundamental wave shows no signs of a peak at 180 Hz suggests that the peak is caused by nonlinear response at 90 Hz.

From the results of Fig. 11, we conclude that the indicated response function in Fig. 12 is accurate to within the uncertainty intervals based on experimental reproducibility up to 150 Hz, subject to the, as yet unknown, limitations of the data analysis. At higher frequencies the indicated response function is subject to the linear DFT interpretation of nonlinear data. Nevertheless the response magnitude apparently does increase with frequency. We know of no better way at this time to explain the increasing amplitude of the time-domain burning-rate data with frequency (Fig. 10). If the linear response magnitude was not increasing with frequency above 150 Hz, the amplitude of $r_b(t)$ should not have increased as it did and should not have exhibited a transition from a nearly linear quasi-sinusoidal response to nonlinear one. To obtain a more accurate quantitative measure of linear response for this propellant above 150 Hz would require a modified burner with a smaller volume amplitude-to-mean ratio.

From the results of Fig. 11, we also observe that it is possible for nonlinear response of a dynamic system (in this case a chemically reacting nonlinear dynamic system) to appear as strong spectral structure in the apparent linear response when the data are interpreted linearly. The response curves of Fig. 12, based on the fundamental input and output components only, exhibit monotonically smooth behavior without strong spectral features such as relatively narrow peaks. On the other hand, the isolated second harmonic component response of Fig. 11 does exhibit strong spectral structure caused by the linear interpretation of nonlinear response data. Some laser-recoil response data have also exhibited a high degree of spectral structure, particularly for composite propellants. It might be well to reexamine such data for the possibility of spectral content being generated by the same mechanism, that is, linear interpretation of nonlinear response data.

Summary

The piston burner shows promise as a linear pressure-coupled response function measuring technique for pressures on the order of 1000 kPa and frequencies of 40–400 Hz, depending on motor size and speed. The response function obtained for a wide-distribution AP propellant shows physically plausible trends with frequency and values for magnitude and phase over the region for which the response was determined to be linear. The reproducibility between tests is good for this type of measurement. The concept of using mass and energy balances to deduce burning rate from pressure–volume data seems viable. Results show that frequency-dependent heat loss is important and must be accounted for in this type of device. Use of the second harmonic was shown to be valuable in assessing linearity of the deduced response. Another useful output of the technique is the nonlinear dynamic burning-rate response data. This data could be very useful in validating combustion models designed to predict the response of composite propellants under unsteady conditions. With incorporation of a variable volume amplitude-to-mean ratio, the piston burner would be capable of measuring both linear and nonlinear dynamic burning response to pressure over an important, low-frequency range at high spectral resolution.

Acknowledgments

Support for this work from the University of Illinois through the Department of Mechanical and Industrial Engineering and the Hermia G. Soo Professorship and U.S. Office of Naval Research (N00014-95-1-1339) is gratefully acknowledged. Theoretical and modeling insight of K. C. Tang of the Center for Simulation of Advanced Rockets is also appreciated.

References

[1]Strand, L. D., and Brown, R. S., "Laboratory Test Methods for Combustion-Stability Properties of Solid Propellants," Nonsteady Burning and Combustion Stability of Solid Propellants, edited by L. De Luca, E. W. Price, and M. Summerfield, Vol. 143, *Progress in Astronautics and Aeronautics*, AIAA, Washington, D.C., 1992, Chap. 17, pp. 689–718.

[2]Cauty, F., "Solid Propellant Combustion Response Function from Direct Measurement Methods: ONERA Experience," *Journal of Propulsion and Power*, Vol. 15, No. 6, 1999, pp. 837–843.

[3]Kudva, G. N., Lee, Y. J., and Litzinger, T. A., "Comparison of Laser and Pressure-Driven Thrust Measurements in the Combustion of an AP/Energetic Binder Propellant," 36th JANNAF Combustion Meeting, Publ. 691, Vol. 1, Chemical Propulsion Information Agency, Columbia, MD, 1999, pp. 575–585.

[4]Beckstead, M. W., and Meredith, K. V., "Examples of Unstable Combustion as Measured in T-Burners," 36th JANNAF Combustion Meeting, Publ. 691, Vol. 1, Chemical Propulsion Information Agency, Columbia, MD, 1999, pp. 539–555.

[5]Blomshield, F. S., "T-Burner Response Analysis Using the SPP/SSP Code," 36th JANNAF Combustion Meeting, Publ. 691, Vol. 1, Chemical Propulsion Information Agency, Columbia, MD, 1999, pp. 557–565.

[6]Culick, F. E. C., "T-Burner Manual," *Chemical Propulsion Information Agency*, Silver Springs, MD, Nov. 1969.

[7]Finlinson, J. C., Stalnaker, R., and Blomshield, F. S., "HMX T-Burner Pressure Coupled Response at 200, 500, and 1000 psi," 36th JANNAF Combustion Meeting, Publ. 691, Vol. 1, Chemical Propulsion Information Agency, Columbia, MD, 1999, pp. 567–574.

[8]Price, E. W., "Experimental Observations of Combustion Instability," Fundamentals of Solid Propellant Combustion, edited by K. K. Kuo and M. Summerfield, Vol. 90, *Progress in Astronautics and Aeronautics*, AIAA, New York, 1984, Chap. 13, pp. 733–790.

[9]Murphy, J. J., and Krier, H., "Linear Pressure Coupled Frequency Response of Heterogeneous Solid Propellants," *Proceedings of the Combustion Institute*, The Combustion Inst., Pittsburgh, PA, Vol. 27, 1998, pp. 2343–2350.

[10]Cardiff, E. H., Pinkham, J. D., and Micci, M. M., "Magnetic Flowmeter Measurement of Pressure-Coupled Response of a Plateau Solid Propellant," *Journal of Propulsion and Power*, Vol. 15, No. 6, 1999, pp. 844–848.

[11]Brewster, M. Q., and Burnside, N. J., "Combustion Response of Wide-Distribution Propellants," *37th JANNAF Combustion Meeting*, Vol. 1, Chemical Propulsion Information Agency, Columbia, MD, 2000, pp. 605–613.

[12]White, F. M., *Viscous Fluid Flow*, McGraw–Hill, New York, 1974, pp. 248, 249.

[13]Heywood, J. B., *Internal Combustion Engine Fundamentals*, McGraw–Hill, New York, 1988, pp. 678, 679.